A Scaling Procedure for Electrically-Excited Synchronous Machines Utilizing Flux and Loss Maps

A Scaling Procedure for Electrically-Excited Synchronous Machines Utilizing Flux and Loss Maps

Federica Graffeo
Dipartimento Energia
Politecnico di Torino
Torino, Italy
federica.graffeo@polito.it

Simone Ferrari
Dipartimento Energia
Politecnico di Torino
Torino, Italy
simone.ferrari@polito.it

Sandro Rubino
Dipartimento Energia
Politecnico di Torino
Torino, Italy
sandro.rubino@polito.it

Silvio Vaschetto
Dipartimento Energia
Politecnico di Torino
Torino, Italy
silvio.vaschetto@polito.it

Gianmario Pellegrino
Dipartimento Energia
Politecnico di Torino
Torino, Italy
gianmario.pellegrino@polito.it

***Abstract*—Electrically-excited synchronous machines are a promising alternative to permanent magnet-based counterparts for traction applications. Besides being rare-earth magnet free, EESMs offer great flexibility of control and high efficiency over a wide range of speed and torque values. This paper introduces a rapid and precise method for scaling the dimensions of electrically-excited machines, leveraging a reference design as a starting point. The proposed procedure utilizes the pre-calculated flux and loss maps of one existing machine to ensure compliance with new peak torque and power, maximum operating speed, voltage, and current specifications, all achieved within minimal computational time. The efficiency map and operating limits of the scaled machine are rapidly derived without necessitating additional finite-element simulations. The efficacy of the procedure is demonstrated by scaling the electrically-excited traction motor of the Renault Zoe to match the performance of the permanent magnet synchronous motor found of the Nissan Leaf drivetrain.**

***Index Terms*—electrically-excited machines, synchronous motors, scaling procedure, traction motors, algorithm design.**

I. Introduction

Electrically-Excited Synchronous Machines (EESMs), also known as wound field/rotor synchronous machines, are gaining popularity as a feasible alternative to Permanent Magnet Synchronous Machines (PMSMs) in transportation applications [1]–[5]. Unlike PMSMs, electrically-excited machines have a *dc*-supplied rotor winding to generate the excitation field. This feature allows for easy adjustment of the excitation field by simply modifying the rotor current, which provides numerous advantages. For instance, EESMs can achieve wide constant power speed ranges while maintaining high efficiencies at high speeds. Moreover, since the machine excitation can be removed in case of fault, concerns related to uncontrolled generation operations are avoided.

The electromagnetic design of EESMs is not a simple task, as the presence of the rotor current introduces an additional degree of freedom that significantly enlarges the design space. Although several design approaches for EESMs can be found in the literature, the majority are either only suitable for generator applications or based on optimization algorithms combined with finite element analysis (FEA), which generally requires significant computational time [5]–[7]. An effective way to rapidly design EESMs is to scale existing machine projects with different dimensions and performance to meet the required targets [8]. Scaling laws are an established procedure that allows for the definition of a new machine design in negligible computational time, albeit bonded to the original machine geometry [9]. The computational efficiency of the scaling process makes this procedure of particular benefit for fast evaluations intended for preliminary technical discussions.

The scaling procedure proposed in this paper extends the work conducted in [8] for PMSMs to EESMs. The scaling process is based on the machine flux maps and has been demonstrated using the EESM motor installed in the Renault Zoe as a reference. The available sample of the EESM motor

Fig. 1. Sample of the Renault ZOE R135 electrically-excited motor.

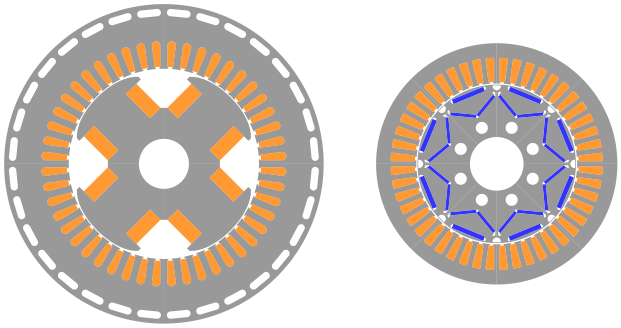

(a) (b)

Fig. 2. Cross section of Zoe motor (a) and Leaf motor (b).

TABLE I
ZOE AND LEAF MOTOR RATINGS.

	Zoe	**Leaf**
Number of pole pairs	2	4
Number of stator slots	48	48
Type of motor	EESM	IPMSM
Winding type	stranded	stranded
Type of cooling	air	liquid
Stator outer diameter	262 mm	198 mm
Stack length	175 mm	150 mm
Turns in series per phase	18	24
Excitation turns	780	-
Rated power	ND	106 kW
Peak power	100 kW	139 kW
Rated torque	ND	208 Nm
Peak torque	245 Nm	290 Nm
Base speed	ND	4000 rpm
Maximum speed	12000 rpm	10000 rpm
Rated phase current	ND	335 Apk
Peak phase current	385 Apk*	480 Apk
DC-link voltage	400 V	375 V
Number of rotor turns per pole	195	-
Maximum excitation current	12.5 A*	-
Rotor resistance @20°C	5.7 Ω	-

**Estimated*
ND = Not Declared

is shown in Fig. 1. The Zoe motor has been scaled to match the performance of the Internal Permanent Magnet Synchronous Machine (IPMSM) used in the Nissan Leaf. The cross sections of both motors are shown in Fig. 2, while their ratings are recollected in Table I. The data of the Zoe motor have been either collected from [10] or obtained from experimental measurements on the available motor sample. The values in Table I indicated as '*Estimated*' have been obtained by calibrating the operative limits computed through the FEA flux and loss maps with those declared in [10].

II. ELECTRICALLY-EXCITED MACHINE MODEL

The voltage equations of electrically-excited machines in steady-state conditions are reported in (1).

$$\begin{cases} v_d = R_s \cdot i_d - \omega \cdot \lambda_q \\ v_q = R_s \cdot i_q + \omega \cdot \lambda_d \\ v_e = R_e \cdot i_e \end{cases} \tag{1}$$

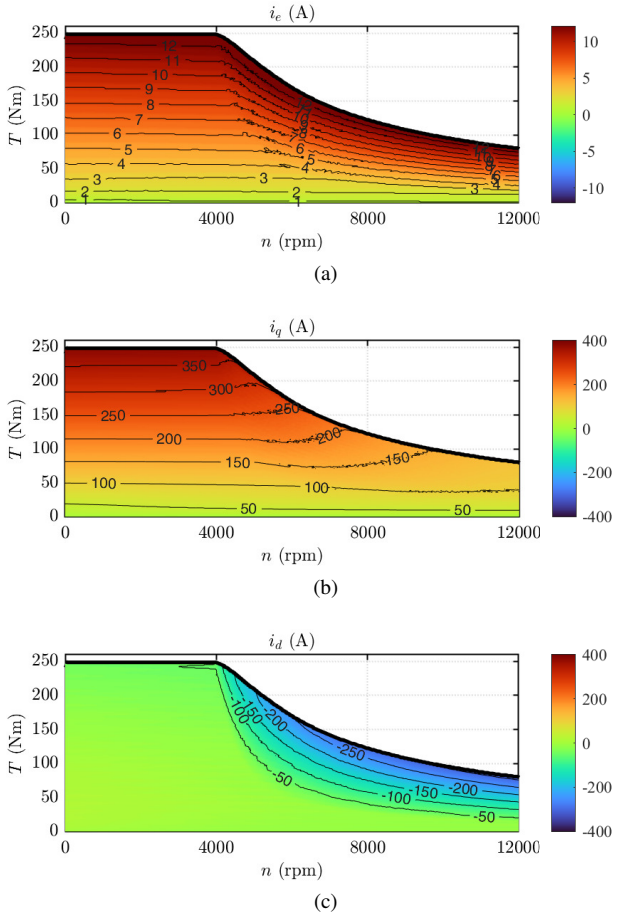

Fig. 3. ZOE maps of the excitation current (a), q-current (b), d-current (c) obtained with the minimum losses strategy.

where v_d, v_q and v_e are the d-, q- and excitation voltages, i_d, i_q and i_e are the d-, q- and excitation currents, λ_d, λ_q are the dq flux linkages, R_s and R_e are the stator and excitation resistances, and ω is the electric pulsation in rad/s.

In this paper, the flux linkages are defined in the form of flux maps as in (2). The bold symbols indicate maps function of the three current components (i_d, i_q, i_e).

$$\begin{cases} \lambda_d = \mathbf{\Lambda}_d(i_d, i_q, i_e) \\ \lambda_q = \mathbf{\Lambda}_q(i_d, i_q, i_e) \\ \lambda_e = \mathbf{\Lambda}_e(i_d, i_q, i_e) \end{cases} \tag{2}$$

The additional degree of freedom introduced by the excitation current enables a variety of control strategies for EESMs. These include maximum efficiency, maximum torque per stator ampere, maximum torque per rotor ampere, zero d-axis current, and unity power factor [11]. For example, Fig. 3 shows the FEA computed maps of the Renault Zoe in terms of excitation, q-, and d-current when the maximum efficiency strategy is applied by minimization of the copper (stator and rotor) and iron losses. The maps refer to a peak stator current of 385A and a rotor current limit of 12.5A. As can be seen, for the considered EESM, the level of excitation current is mainly changed according to the torque request. On the contrary,

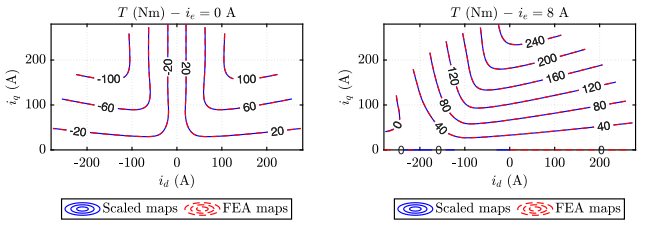

(a) (b)

Fig. 4. Torque maps obtained by the scaling equations and FEA-computed maps of the scaled motor for different rotor currents.

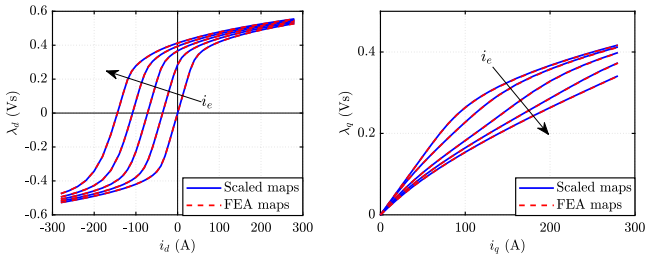

(a) (b)

Fig. 5. *dq*-saturation curves of the scaled motor obtained by the scaling equations and FEA-computed maps.

the flux weakening is performed by injecting an increasingly negative d-axis current. However, an ideal flux-weakening curve can be pursued with the maximum power maintained up to the maximum speed by controlling the motor with a stator current equal to the motor's characteristic current. In EESM, the characteristic current is a function of the excitation current and is defined as the current that compensates for the rotor flux linkage created by the excitation circuit, as in (3).

$$i_{ch}(i_e) = i_d|_{\mathbf{\Lambda}_d(i_d,i_q=0,i_e)=0} \tag{3}$$

One of the advantages of EESMs is the possibility to control the characteristic current acting on the excitation current, obtaining a flat power profile for all the loads without efficiency detriment.

III. Scaling Rules Definition

The scaling process is based on four scaling factors defined in (4). The scaling factors are defined as the ratio between the quantities of the scaled machine and the quantities of the baseline machine, denoted with the subscript 0. The scaling factors can modify the radial dimensions (k_D), the axial dimension (k_L), the number of stator turns in series per phase (k_N), and the number of rotor turns (k_E). In the definition, D denotes the stator outer diameter, L the stack length, N_s the number of stator turns in series per phase and N_e the number of turns of the excitation winding.

$$\begin{cases} k_D = \frac{D}{D_0} \\ k_L = \frac{L}{L_0} \\ k_N = \frac{N_s}{N_{s,0}} \\ k_E = \frac{N_e}{N_{e,0}} \end{cases} \tag{4}$$

The scaling rules of electrical machines are well-known [9], but are typically adopted and implemented just on the rated working point of the motor. However, the scaling rules can be extended on the entire flux map of the motor, dramatically reducing the motor's identification time.

A. Scaling of Flux Maps

Under the assumption of maintaining the same field distribution in the motor cross-section, the linear current density must be kept constant. In this case, the flux linkages can be scaled as:

$$\frac{\mathbf{\Lambda}_d}{\mathbf{\Lambda}_{d,0}} = k_D \cdot k_L \cdot k_N \tag{5}$$

$$\frac{\mathbf{\Lambda}_q}{\mathbf{\Lambda}_{q,0}} = k_D \cdot k_L \cdot k_N \tag{6}$$

$$\frac{\mathbf{\Lambda}_e}{\mathbf{\Lambda}_{e,0}} = k_D \cdot k_L \cdot k_E \tag{7}$$

where $\mathbf{\Lambda}_d$, $\mathbf{\Lambda}_q$ and $\mathbf{\Lambda}_e$ are the 3D matrices of flux linkages of the scaled machine, function of (i_d, i_q, i_e) and $\mathbf{\Lambda}_{d,0}$, $\mathbf{\Lambda}_{q,0}$ and $\mathbf{\Lambda}_{e,0}$ are the 3D matrices of flux linkage of the initial motor, function of $(i_{d,0}, i_{q,0}, i_{e,0})$. In order to keep the linear current density constant, also the current maps (that are the coordinates of the flux maps) must be scaled as:

$$\frac{\mathbf{I}_d}{\mathbf{I}_{d,0}} = k_D \cdot k_N^{-1} \tag{8}$$

$$\frac{\mathbf{I}_q}{\mathbf{I}_{q,0}} = k_D \cdot k_N^{-1} \tag{9}$$

$$\frac{\mathbf{I}_e}{\mathbf{I}_{e,0}} = k_D \cdot k_E^{-1} \tag{10}$$

For simplicity, the end-winding inductance is assumed to be negligible. Once flux linkages maps and current maps are scaled, the electromagnetic torque map can be scaled as:

$$\frac{\mathbf{T}}{\mathbf{T}_0} = k_D^2 \cdot k_L \tag{11}$$

As an example, the torque maps at two different excitation currents are reported in Fig. 4, while the d-axis flux at zero q-current and the q-axis flux at zero d-current are reported in Fig. 5 for different rotor currents. The plots compare the maps obtained by the described scaling equations (solid blue contour) with the FEA-computed maps of the scaled motor (dashed red contour).

B. Scaling of Loss Components

Three terms of loss must be considered and scaled, namely stator copper loss $P_{J,s}$, excitation copper loss $P_{J,e}$ and iron loss P_{Fe} (both rotor and stator). Note that just the losses refing to sinusoidal supply are considered. Winding AC loss are not part of the scaling process at the moment, while PWM loss are not included because of the dependency of the drive system. Both loss terms must be re-computed after scaling. A common and general approach to model iron loss is to express them as a function of the currents in a similar framework of flux maps, as done for PMSMs in [12]. The only difference with flux maps is the dependency of the rotor speed ω_r: indeed, iron loss maps are computed at constant speed and then scaled according to the considered formulation (Steinmetz, Bertotti or others). As iron loss are proportional to the iron volume, iron loss maps can be scaled as:

$$\frac{\mathbf{P}_{Fe}}{\mathbf{P}_{Fe,0}} = k_D^2 \cdot k_L \tag{12}$$

On the other hand, the copper loss are mainly function of the currents and the resistance of the respective circuits. Dealing with stator copper loss, neglecting the AC effects, the stator resistance is scaled as:

$$\frac{R_s}{R_{s,0}} = \frac{k_N^2}{k_D^2} \cdot \left(k_L \cdot \frac{L_0}{L_0 + L_{ew,0}} + k_D \cdot \frac{L_{ew,0}}{L_0 + L_{ew,0}} \right) \tag{13}$$

where $L_{ew,0}$ is the end-winding length, which is proportional to k_D. Once the phase resistance is scaled and the *dq* currents are re-mapped, the stator copper loss can be computed as:

$$\mathbf{P}_{Js} = \frac{3}{2} \cdot R_s \cdot (\mathbf{I}_d \odot \mathbf{I}_d + \mathbf{I}_q \odot \mathbf{I}_q) \tag{14}$$

where the symbol $\odot$ identifies the element-wise product between matrices. The excitation copper loss can be computed in a similar way. The excitation resistance R_e is scaled as:

$$\frac{R_e}{R_{e,0}} = \frac{k_E^2}{k_D^2} \cdot \left(k_L \cdot \frac{L_0}{L_0 + L_{e,ew,0}} + k_D \cdot \frac{L_{e,ew,0}}{L_0 + L_{e,ew,0}} \right) \tag{15}$$

Then, the excitation copper losses are recomputed as:

$$\mathbf{P}_{Je} = R_e \cdot (\mathbf{I}_e \odot \mathbf{I}_e) \tag{16}$$

C. Scaling of Maximum Operating Speed

The maximum motor speed is related to the centrifugal stress that the rotor can sustain. As explained in [8], the maximum Von Mises stress in the rotor is proportional to $D^2 \cdot n_{max}^2$. So the stress scaling rule results:

$$\frac{\sigma_{max}}{\sigma_{max,0}} = k_D^2 \cdot \left(\frac{n_{max}}{n_{max,0}} \right)^2 \tag{17}$$

Assuming that the material of the scaled motor does not change, the maximum stress of the scaled motor must be the same as the initial motor, so $\sigma_{max} = \sigma_{max,0}$. With this condition, the scaling rule for the maximum speed results:

$$\frac{n_{max}}{n_{max,0}} = k_D^{-1} \tag{18}$$

IV. Proposed Scaling Procedure

In the proposed procedure, the inverter limits (DC link voltage and peak phase current) are imposed, and the operating point of the motor is automatically adapted to adjust to these inputs and account for all the non-linearities. The steps of the scaling procedure are:

1) Radial Scaling: radial scaling is the only factor affecting the maximum rotor speed. The radial scaling factor k_D can be computed by imposing the maximum speed, as in (18) or by imposing a target outer diameter, in which case the maximum speed is re-computed.
2) Axial and Stator Turns Scaling: once k_D is computed, the axial and stator turns scaling factors k_L and k_N are computed thanks to a scaling plane in (L, N_s), imposing the maximum inverter current and the DC-link.
3) Excitation Circuit Scaling: the last step of the scaling process deals with the excitation circuit. From the (L, N_s) plane, the excitation ampere-turns are derived, so the number of turns of the excitation circuit is retrieved from the maximum excitation voltage.

A. (L, N_s) Scaling Plane

The core of the scaling procedure is the (L, N_s) scaling plane, adopted to identify the two related scaling factors (k_L and k_N). The scaling map refers to the base speed and peak torque point, that will be computed for each scaled motor of the plane. For each (L, N_s) point, the flux maps of the reference EESM are scaled. Then, the operating point is identified by assuming an excitation control that sets the characteristic current equal to the maximum stator current. In this way, an ideal field-weakening profile will be obtained, and the excitation ampere-turns can be computed. Note that for EESM, among the several control options, the selected method is not too far from the maximum efficiency control but is way easier to implement in the preliminary design stage when the scaling process is adopted. The final scaling map, computed with the same inverter limits of the target motor (Leaf), is reported in Fig. 6a. The plane reports peak torque and base speed function of the stack length L and the number of turns in series per phase N_s. Peak torque and base speed have opposite trends: the torque increases going from bottom-left to top-right, while the base speed has the opposite trend. The flux and loss maps and resistances can be scaled thanks to the previously presented scaling rules. To help the motor selection and further reduce the valid area in the (L, N_s) plane, additional quantities can be reported on the scaling plane as the excitation ampere-turns (needed to cope the characteristic current with the maximum stator current) and the specific copper loss, reported as example in Fig. 6b and Fig. 6c.

B. Scaling of the Excitation Circuit

In order to determine the appropriate number of turns for the excitation winding, it is necessary to consider the available voltage of the rotor. This is because the voltage of the rotor will ultimately determine the amount of current that can be induced in the excitation winding. As a result, the number of

turns in the excitation winding must be scaled appropriately to ensure that it can produce the required magnetic field while operating within the limits of the available rotor voltage. The application of Ohm's law to the rotor circuit determines the scaling rule of the excitation turns:

$$k_E = k_D^2 \cdot \frac{1}{A} \cdot \frac{V_e}{V_{e,0}} \cdot \frac{N_{e,0} \cdot I_{e,max,0}}{N_e \cdot I_{e,max}} \tag{19}$$

In equation (19), the value of A is expressed as in (20).

$$A = k_L \cdot \frac{L_0}{L_0 + L_{e,ew,0}} + k_D \cdot \frac{L_{e,ew,0}}{L_0 + L_{e,ew,0}} \tag{20}$$

For the computation of k_E, the value of the excitation ampere-turns of the scaled motor, i.e. the product $N_e \cdot I_{e,max}$, is established through the (L, N_s) scaling plane. The value of the rotor turns, and the maximum excitation current of the baseline motor are known and listed in Table I. Concerning the ratio $V_e/V_{e,0}$, the definition depends on the available rotor voltage. If this information is missing, then the same percentage of rotor voltage with respect to the DC link can be assumed in the motor's scaling process. Another option is to consider that the value of the rotor voltage remains constant with respect to the baseline motor, hence assuming $V_e/V_{e,0} = 1$ as a first approximation.

V. Case Studies

To demonstrate the proposed scaling procedure, the Zoe motor is scaled to match the peak specs of the Leaf motor. The different cooling types, i.e. forced air for the Zoe and water-jacket for the Leaf, represent a critical non homogeneity when comparing the two motors, leading to scaled EESMs of larger volumes with respect to the liquid-cooled Leaf PMSM. Nevertheless, the validity of the described scaling procedure remains intact.

A. Radial Scaling

According to the procedure described in the previous section, the first step of the motor scaling is to identity the radial scaling factor k_D. In this case, the maximum speed is pursued, and the radial scaling is computed according to (18). With the benchmark data, it becomes:

$$k_D = \frac{n_{max,Zoe}}{n_{max,Leaf}} = \frac{12000}{10000} = 1.2 \tag{21}$$

Note that the diameter of the scaled motor will be larger than the baseline motor. The comparison with the Zoe motor follows from the different maximum speeds, while the comparison with the Leaf motor is more complex since a different number of poles is considered. If the rotor diameters of the scaled EESM and the Leaf motor are compared, the difference is not crucial, while the structural problem for EESM and IPMSM is quite different and needs further investigation.

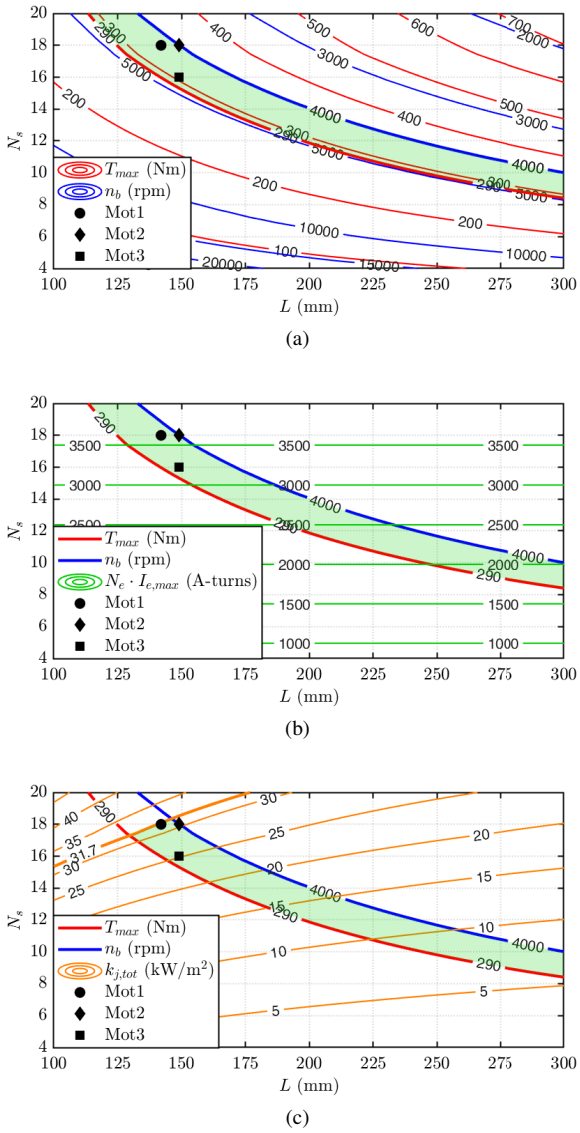

Fig. 6. Scaling map for the considered benchmark case: a) torque and speed versus stack length and stator turns, b) excitation ampere-turns versus stack length and stator turns and c) specific loss function of stack length and stator turns.

B. Axial and Stator Turns Scaling

The scaling plane is reported in Fig. 6. The main plane reports torque and base speed at the maximum inverter limits and computing the excitation ampere-turns $N_e \cdot i_e$ (reported in Fig. 6b) in order to have the characteristic current equal to the maximum stator current. The green-shaded area identifies all the motors on the scaling plane that fulfil both maximum torque and base speed requirements (reported with bold lines). The final motors must be identified inside this area. To slightly reduce the preferred area, the specific copper loss $k_{j,tot}$ can be considered. It is defined as the total copper loss at rated windings temperature divided by the stator outer surface. Even if this index suffers from some approximations, it is representative of the cooling system's capability. The specific

TABLE II
COMPARISON BETWEEN THE TARGET MOTOR (LEAF) AND THE SCALED MOTORS.

	Leaf	**Mot1**	**Mot2**	**Mot3**
Number of pole pairs	4	2	2	2
Number of stator slots	48	48	48	48
Type of motor	IPMSM	EESM	EESM	EESM
Type of cooling	liquid	air	air	air
Peak phase current (Apk)	480	480	480	480
DC-link voltage (V)	375	375	375	375
Stator diameter (mm)	198	314	314	314
Stack length	150	142	149	149
Turns in series per phase	24	18	18	16
Rotor turns per pole	-	211	205	223
Excitation (A-turns)	-	3510	3510	3224
Peak torque (Nm)	290	330	346	305
Base speed (rpm)	4000	4200	4000	4600
Maximum speed (rpm)	10000	10000	10000	10000
Stator winding temp. (°C)	150	150	150	150
PM temp. (°C)	100	-	-	-
Rotor winding temp. (°C)	-	150	150	150

losses are reported in Fig. 6c and the value of the Zoe motor is reported with a bold line, reducing the green area. To demonstrate the scaling process, three motors are selected from the (L, N_s) plane. The most convenient area for selection is on the left side of the green area, being characterized by feasible motors with the smallest volumes. The motors are thus chosen accordingly and considering only solutions with an integer number of stator turns. Figure 6 reports the selected motors, while their main characteristics are listed in Table II. The preferred motor is Mot1 (the one with the shortest stack), while the other two motors are selected to show how the motors change based on the (L, N_s) point.

C. Excitation Turns Scaling

From the (L, N_s) plane, the value of the ampere-turns corresponding to the maximum rotor current is identified for the three motors and reported in Table II. For the computation of the scaling factor k_E, the rotor voltage of the scaled motors is assumed equal to that of the reference machine. The latter has been computed as the product of the maximum rotor current and the rotor winding resistance. Once the value of k_E is obtained using (19), the number of rotor turns per pole N_e of the scaled motors can be computed. The resulting values are listed in Table II. The corresponding excitation current can be simply obtained by dividing the ampere-turns by rotor turns per pole N_e.

D. Scaled Motors Comparison

The three scaled EESMs are compared to the Leaf PMSM in Table II and Fig. 7. Expectedly, the three scaled EESMs feature a larger outer diameter with resepct to the Leaf motor, with similar stack length. The larger active volume relates to both the superior torque density figures of PMSMs and the different adopted cooling techniques. As said in Section V, a fair comparison should consider motors with the same cooling capability.

The three scaled motors have slightly higher torques and base speeds than the Leaf motor, which is consistent with the

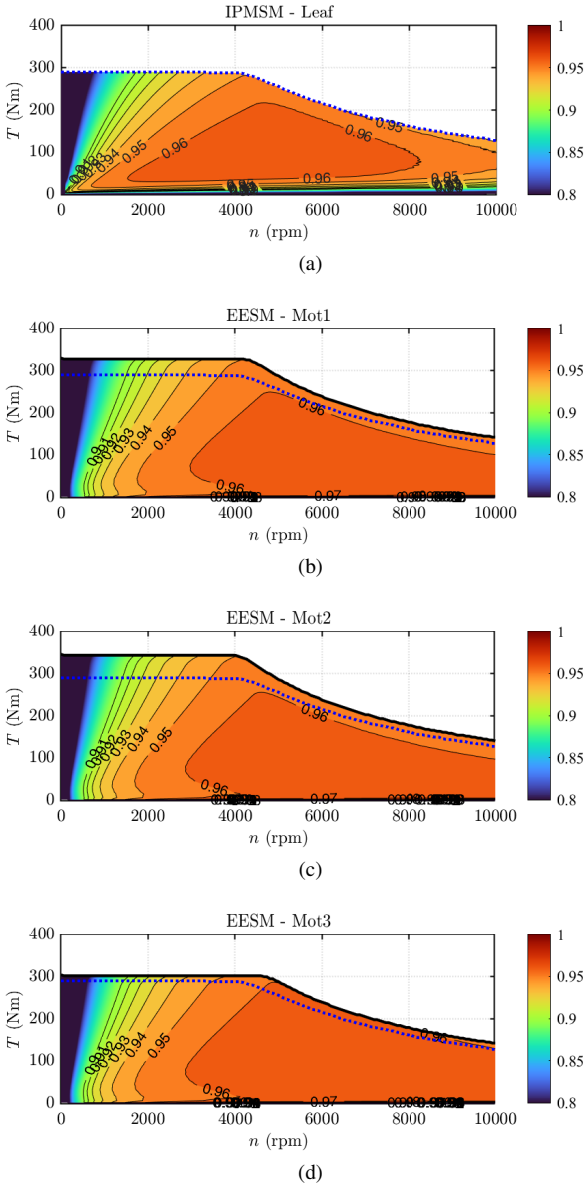

Fig. 7. Efficiency maps of Leaf (a) and the three scaled EESM motors (b,c,d), computed at the inverter limits and the temperatures reported in Table II.

data of the (L, N_s) scaling plane. Figure 7 shows the efficiency maps of the Leaf and scaled motors, considering iron losses (both in the stator and the rotor), stator copper losses and either PM losses or rotor copper losses, depending on the motor type [13], [14]. Please, note that all the mentioned loss components are considered with sinusoidal supply. AC loss related to skin and proximity effects in the conductors and PWM loss are disregarded in the comparison, as well as the mechanical loss. In addition, the maps of the scaled motors report, in dashed blue lines, the operative limits of the Leaf motor in order to highlight the differences between the scaled EESM and the target IPMSM. The computed maps confirm the peak torque and base speed values of the scaled motors. It can be noted that the three EESMs reach higher efficiency values than the Leaf motor. Moreover, the efficiency of the

IPMSM tends to decrease at high speeds, while the EESMs succeed in maintaining high efficiency values for the whole speed range. Indeed, the flux weakening in IPMSM requires injecting negative d-currents to compensate for the magnetic flux generated by the permanent magnets, leading to efficiency detriment. In EESMs, although negative d-currents are still used for flux weakening operations (see Fig.3c), the value of the magnetic flux to be compensated is not fixed and is regulated by the excitation current, resulting in better machine exploitation.

VI. Conclusion

A fast scaling procedure is proposed for the preliminary design of EESMs considering the peak motor performance. The workflow relies on applying fast scaling rules to flux and loss maps of EESMs, allowing for the accurate estimation of the output characteristics of the new motor. This approach provides direct access to the flux and loss maps of the scaled motor without requiring any additional FEA simulation. This is particularly useful in the case of electrically-excited machines, where the computational burden of the flux maps is significantly increased due to the presence of a third simulation variable, i.e. the rotor current. Moreover, the flux and loss maps of the scaled motor can be further evaluated for efficiency maps computation and control algorithm implementation. A graphical method is introduced for selecting the best trade-off between stack length and stator number of turns, considering the other key design outputs. The procedure is demonstrated by scaling the EESM of the Renault Zoe to match the peak performance of the IPMSM motor equipping the Nissan Leaf. Three motors are selected from the proposed (L, N_s) scaling plane and compared to the original Leaf motor to showcase the proposed workflow operation. Last, the EESMs and IPMSM efficiency maps are compared, highlighting the efficiency advantages of EESM compared to IPMSM at medium-high speeds.

References

[1] H.-J. Park and M.-S. Lim, "Design of High Power Density and High Efficiency Wound-Field Synchronous Motor for Electric Vehicle Traction," *IEEE Access*, vol. 7, pp. 46 677–46 685, 2019.

[2] "Specifications. (from 9/2021 on). BMW iX3." accessed: 29-March-24. [Online]. Available: https://www.press.bmwgroup.com/global/article/attachment/T0338848EN/524017

[3] "ZF makes magnet-free electric motor uniquely compact and competitive," accessed: 29-March-24. [Online]. Available: https://press.zf.com/press/en/releases/release_60480.html

[4] C. Stancu, T. Ward, K. M. Rahman, R. Dawsey, and P. Savagian, "Separately excited synchronous motor with rotary transformer for hybrid vehicle application," *IEEE Transactions on Industry Applications*, vol. 54, no. 1, pp. 223–232, 2018.

[5] F. Graffeo, S. Vaschetto, A. Tenconi, and A. Cavagnino, "Fast sizing procedure for salient-pole wound field synchronous motors for transportation electrification," in *2023 IEEE International Electric Machines & Drives Conference (IEMDC)*, 2023, pp. 1–7.

[6] T. d. P. M. Bazzo, V. d. O. Moura, and R. Carlson, "A step-by-step procedure to perform preliminary designs of salient-pole synchronous generators," *Energies*, vol. 14, no. 16, 2021. [Online]. Available: https://www.mdpi.com/1996-1073/14/16/4989

[7] D. C. Ludois and I. Brown, "Brushless and Permanent Magnet Free Wound Field Synchronous Motors for EV Traction," University of Wisconsin -Madison, Tech. Rep. DOE-Wisconsin–6849, 1349258, Mar. 2017. [Online]. Available: http://www.osti.gov/servlets/purl/1349258/

[8] G. Dilevrano, P. Ragazzo, S. Ferrari, G. Pellegrino, and T. Burress, "Magnetic, thermal and structural scaling of synchronous machines," in *2022 IEEE Energy Conversion Congress and Exposition (ECCE)*, 2022, pp. 1–8.

[9] S. Stipetic, D. Zarko, and M. Popescu, "Ultra-fast axial and radial scaling of synchronous permanent magnet machines," *IET Electric Power Applications*, Aug. 2016.

[10] "RENAULT ZOE E-TECH 100% electric," accessed: 29-March-24. [Online]. Available: https://cdn.group.renault.com/ren/gb/transversal-assets/brochures/mobile-brochure-tech-spec/mobile-tech-spec-zoe.pdf

[11] F. Graffeo, "Modeling and design of wound-field synchronous machines for transportation applications," Ph.D. dissertation, Politecnico di Torino, 2023.

[12] S. Ferrari, P. Ragazzo, G. Dilevrano, and G. Pellegrino, "Flux and loss map based evaluation of the efficiency map of synchronous machines," *IEEE Transactions on Industry Applications*, vol. 59, no. 2, pp. 1500–1509, 2023.

[13] S. Ferrari, G. Pellegrino, and et al., "SyR-e: Synchronous Reluctance (machines) - evolution." [Online]. Available: www.github.com/SyR-e/syre_public

[14] D. Meeker, "FEMM: Finite Element Method Magnetics." [Online]. Available: www.femm.info

Biographies

Federica Graffeo (S'20-M'24) received the B.Sc. degree in Energy Engineering from Università degli Studi di Palermo (Italy) in 2017, the M.Sc. and Ph.D. degree in Electrical Engineering from Politecnico di Torino (Italy) in 2020, and 2023, respectively. She is currently Assistant Professor with Dipartimento Energia "G. Ferraris," Politecnico di Torino. She serves as a reviewer for some IEEE Transactions and international conferences. Her main research interests include electromagnetic and thermal design of synchronous electrical machines for transportation applications, with a particular focus on wound field synchronous motors.

Simone Ferrari (S'17-M'20) received the Ph.D. degree "cum laude" in 2020 from Politecnico di Torino, where he is currently an Assistant Professor. From July to December 2018, he was a Visiting Scholar at North Carolina State University, Raleigh, NC, USA. Between 2021 and 2023 he was the responsible of the TEST-eDRIVE infrastructure, a test rig for EV drive applications managed by Politecnico di Torino and the Power Electronics Innovation Center. He is one of the authors of SyR-e, an open-source environment for the design, analysis and modeling of synchronous reluctance and permanent magnet machines. His research interests include electrical machine design and testing, with a focus on synchronous reluctance and permanent magnet machines and propulsion applications.

Sandro Rubino (S'16, M'18) received the M.Sc. and Ph.D. degrees in Electrical Engineering from Politecnico di Torino, Torino, Italy, in 2014 and 2019, respectively. He is currently Assistant Professor with Dipartimento Energia "G. Ferraris," Politecnico di Torino. He serves as a reviewer for some IEEE Transactions and international conferences. His main research interests include power electronics, modeling, and control of multiphase electrical machines and high-performance *ac* motor drives. Dr Rubino is an Associate Editor of IEEE Transactions

on Industry Applications on behalf of the Industrial Drive Committee of the IEEE Industry Applications Society. He was the recipient of two paper awards from the Industrial Drives Committee of the IEEE Industry Applications Society and two Ph.D. thesis awards from the IEEE Power & Energy Society Italy Chapter and the IEEE Industrial Electronics Society Italy Chapter, respectively.

Silvio Vaschetto (S'10–M'13–SM'19) received the M.Sc. and Ph.D. degrees in electrical engineering from the Politecnico di Torino, Italy, in 2007 and 2011, respectively. He then joined ABB IEC LV Motors Technology Center, Vittuone, Italy as R&D engineer. From 2012 to 2014 he was with Magna Electronics Italy, as Electromagnetic Simulation and Motor Design Engineer. He is currently an Associate Professor at the Energy Department "G. Ferraris", Politecnico di Torino. His research interests include electromagnetic design, thermal analysis, and energetic behavior of electrical machines for transportations and high-performance applications. He is an Associate Editor for IEEE TRANSACTIONS ON INDUSTRY APPLICATIONS, IEEE TRANSACTIONS ON ENERGY CONVERSION and Special Issues Editor for IET ELECTRIC POWER APPLICATIONS JOURNAL.

Gianmario Pellegrino (F' 22, SM '13, M'06) is Professor of Power Converters, Electrical Machines and Drives at Politecnico di Torino, Turin, Italy. He was a visiting fellow at Aalborg University, the University of Nottingham, and the University of Wisconsin-Madison. Dr. Pellegrino is author of the open-source platform SyR-e for the design of electrical motors and drives, constantly developed and validated in the context of collaborations with the industry, and widely adopted world-wide. Dr. Pellegrino is an IEEE Fellow, an Associate Editor for the IEEE Transactions on Industry Applications and the recipient of the 8th Grand Nagamori Award. He co-authored 60+ IEEE journal papers and eight patents and received nine Best Paper Awards. He is a founding member of the Power Electronics Interdepartmental Center (PEIC) of Politecnico di Torino, and a member of the Advisory Board of PCIM Europe.